

October 2008

Numerical analysis of the spectral response of an NSOM measurement

Edward C. Kinzel

Purdue University, kinzele@purdue.edu

Xianfan Xu

Birck Nanotechnology Center, School of Materials Engineering, Purdue University, xxu@purdue.edu

Follow this and additional works at: <http://docs.lib.purdue.edu/nanopub>

Kinzel, Edward C. and Xu, Xianfan, "Numerical analysis of the spectral response of an NSOM measurement" (2008). *Birck and NCN Publications*. Paper 112.

<http://docs.lib.purdue.edu/nanopub/112>

This document has been made available through Purdue e-Pubs, a service of the Purdue University Libraries. Please contact epubs@purdue.edu for additional information.

Numerical analysis of the spectral response of an NSOM measurement

E.C. Kinzel · X. Xu

Received: 29 June 2008 / Published online: 30 August 2008
© Springer-Verlag 2008

Abstract Near-field Scanning Optical Microscopy (NSOM) is a powerful tool for investigating optical field with resolution greater than the diffraction limit. In this work, we study the spectral response that would be obtained from an aperture NSOM system using numerical calculations. The sample used in this study is a bowtie nanoaperture that has been shown to produce concentrated and enhanced field. The near- and far-field distributions from a bowtie aperture are also calculated and compared with what would be obtainable from a NSOM system. The results demonstrate that it will be very difficult to resolve the true spectral content of the near-field using aperture NSOM. On the other hand, the far-field response may be used as a guide to the near-field spectrum.

PACS 07.79.Fc · 68.37.Uv · 42.79.Gn

1 Introduction

Near-field Scanning Optical Microscopy (NSOM) is a powerful tool for peering beyond the diffraction limit. It plays an increasingly important role for the investigation of nanoscale devices that manipulate light on length scales that do not effectively couple into the far-field such as sub-wavelength apertures and plasmonic structures [1, 2]. One of the principle advantages of NSOM is the potential to resolve the spectral content in the near-field in addition to resolving optical signals with high spatial resolution.

In order to measure the near-field, a probe must scatter the evanescent waves into the far-field where they can be measured by a photo sensor such as a photo multiplier tube. These near-field probes are constructed with nanoscale feature sizes, often using standard micro and nanofabrication techniques. The dimensions of the probe permit a very small interrogation volume. Because the position of the probe can be very accurately controlled relative to the specimen of interest, NSOM can spatially resolve optical signals as well as topography of a sample.

In many applications the spectral response of the nanoscale specimen is of interest. The purpose of this paper is to evaluate how NSOM measurements can reveal the spectral information. There exist possible differences between the actual near-field and the NSOM measured signals, which can be understood from Bethe's theory [3]. The Bethe's theory analytically examined the light transmission through a subwavelength circular aperture in a perfectly conducting screen. For illumination by a normally incident plane wave, the ratio of the diffracted energy to the incident energy, T , through a circular hole of radius r is given by a first order approximation as

$$T \approx \frac{1024\pi^2 r^4}{27 \lambda^4}. \quad (1)$$

It is expected that signal passing through such an aperture of an NSOM probe will have longer wavelengths more significantly attenuated, therefore distorting the spectral distribution of the near field.

A nanoscale bowtie aperture is selected as the sample in this work whose near- and far-field are to be studied. The bowtie aperture is a type of ridge waveguide, and together with other nanoscale apertures, are of current interest as a means of producing a nanoscale near-field spot [4–7]. Its

E.C. Kinzel · X. Xu (✉)
School of Mechanical Engineering and Birck Nanotechnology
Center, Purdue University, West Lafayette, IN 47907, USA
e-mail: xxu@ecn.purdue.edu

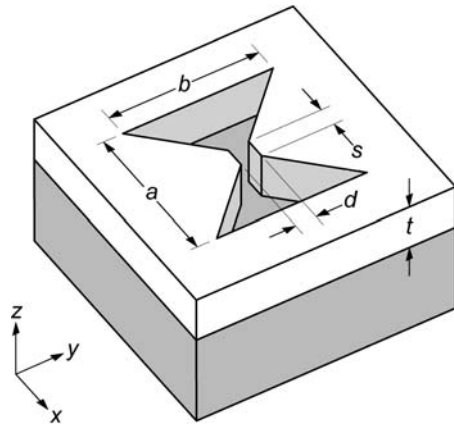


Fig. 1 Schematic of bowtie aperture

Table 1 Cutoff wavelengths for different outline dimensions of bowtie waveguide

a [nm]	125	150	175	200
λ_1 [nm]	410.5	516.5	625.4	736.9

optical throughput is much higher than a similarly sized circular or square aperture because its cutoff wavelength is much longer [4]. Loading a waveguide with ridges is a well known approach in microwave engineering for raising the cutoff wavelength and increasing the useful operational range [8, 9]. A schematic of a nanoscale bowtie aperture studied is shown in Fig. 1. A thin metallic film (aluminum in this study) is evaporated on top of a dielectric substrate which is typically quartz. A plane wave polarized in the y -direction is incident from the bottom of the substrate, propagating in z -direction. For the work presented in this paper, the aperture is defined by a 25×25 nm gap ($s = d = 25$ nm) and in a metal film with thickness of 150 nm ($t = 150$ nm). These dimensions are selected because they are representative of real apertures milled using a focused ion beam (FIB) in aluminum films evaporated onto quartz substrates. By selecting the outer dimensions, a and b , the resonant wavelength of the aperture can be tuned. Table 1 shows the numerically calculated cutoff wavelengths for the first propagating mode of the various sized waveguides ($a = b$ with $s = d = 25$ nm).

Figure 2(a) shows the schematic of an NSOM probe formed by milling a circular hole of radius r onto the apex of the pyramidal tip, which is a typical tip used in an atomic force microscope (AFM). The AFM probe is formed by evaporating a thin (120 nm) aluminum coating onto a silicon nitride core. Detail description of the NSOM probe fabrication was given elsewhere [1]. When using such an NSOM probe for measuring the near field response of a sample (a bowtie aperture in this case), the aperture is illuminated from the bottom through the

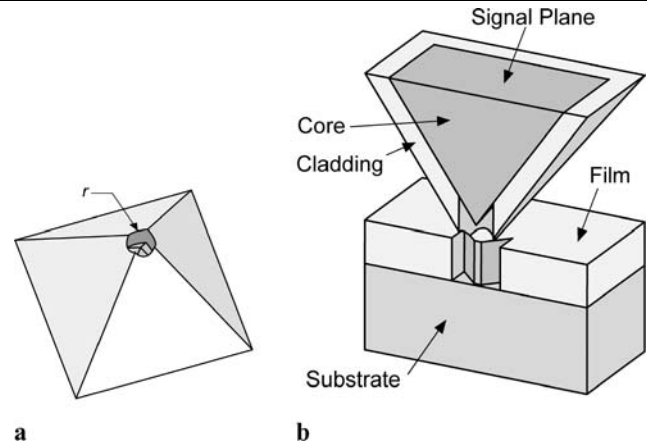


Fig. 2 Problem definition: (a) probe geometry and (b) Probe scanning bowtie nanoaperture

quartz substrate by a plane wave polarized in the y -direction and propagating along the z -axis. The signal is collected by focusing a microscope objective onto the exit of the NSOM probe. The probe can be in intimate contact with the specimen surface during the NSOM measurement.

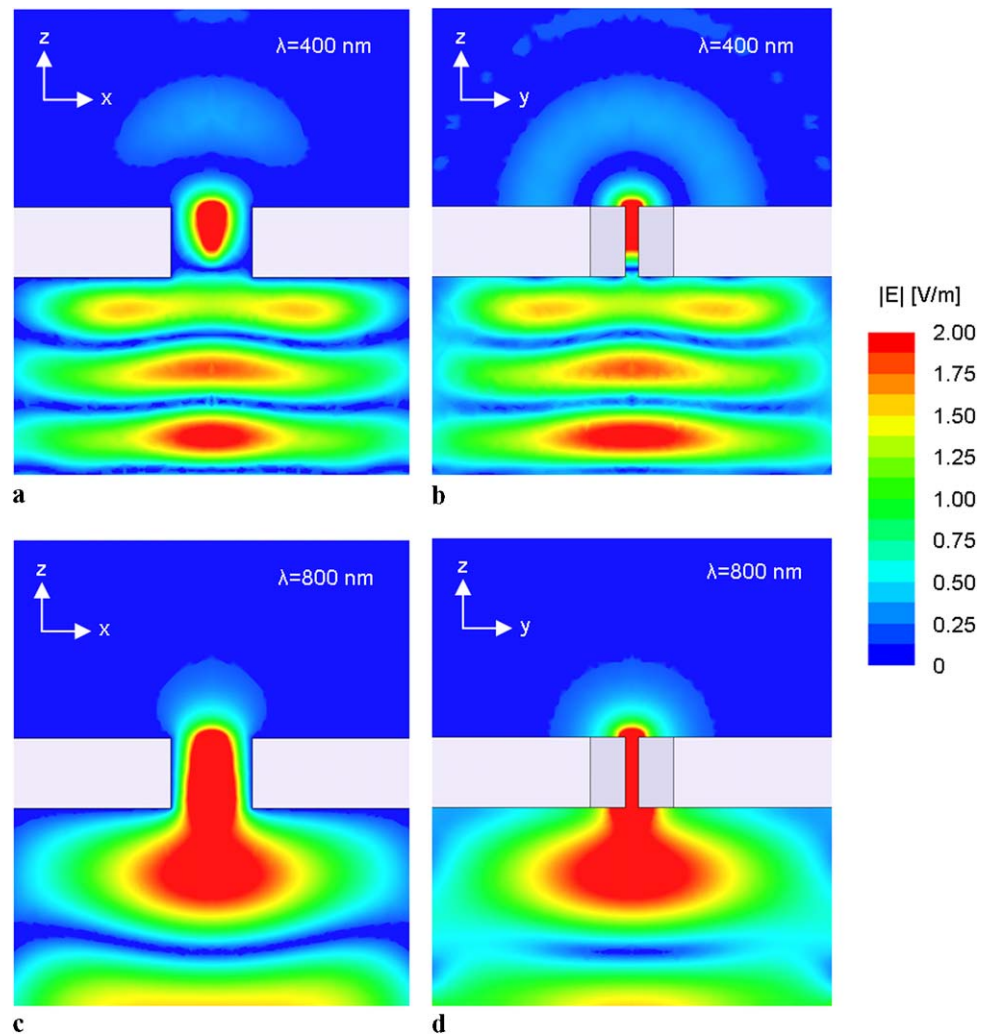
In this study, the near-field and far-field distributions of the bowtie aperture are computed. The field from the bowtie aperture collected by the NSOM probe is also calculated and compared with the near-field and far-field results. To isolate the geometric response from the material response, the problem is first addressed by modeling the metal surfaces as a perfect electrical conductor (PEC). The ability of the NSOM probe to resolve the resonant peaks is analyzed numerically along with the effect of the radius of the NSOM probe aperture. The calculations are then expanded to consider the properties of a real metal, aluminum.

2 Numerical analysis

2.1 Simulation setup

This study uses HFSS (Version 10.1), a software package based on the finite element method (FEM) in the frequency domain to solve the Maxwell's equations [10]. This software package has been used previously to investigate nanoscale 'C' waveguide apertures [6], including a validation of its applicability to the length scale using real metal properties in the optical frequency range. The computational domain is discretized using tetrahedral elements. Edge basis functions and second-order interpolation functions are expanded over the elements [6, 10]. Once the field distribution has been solved, the mesh is refined to add more elements in regions where the intensities or gradients are high. This iterative approach is very useful because the mesh needs to be

Fig. 3 E-field magnitude for 150 nm thick PEC bowtie aperture ($a = b = 150$ nm) under plane wave illumination (wave polarized in y -direction) for $\lambda = 400$ nm in the (a) H plane, (b) E plane, and $\lambda = 800$ nm in the (c) H plane and (d) E plane

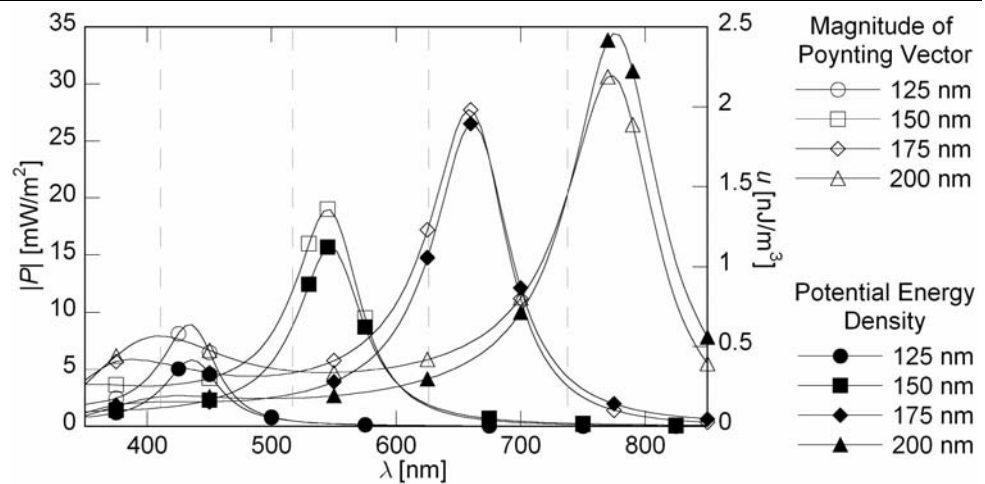


very dense around the aperture and sparser where the fields are weak, which permits the boundaries to be placed further from the strongly radiating features, and is in contrast to finite difference time domain (FDTD) techniques, which normally do not provide as much flexibility in their grids. Another advantage of using FEM in the frequency domain is that the optical properties for the various materials can be readily implemented as a function of wavelength, whereas to simulate these metals in the time-domain, the Debye model is typically used which results in non-trivial errors if it is not properly fit to the wavelength range of interest. Operating in the frequency-domain also simplifies the calculation of the far-field data, because the time-domain solution data requires conversion (Fourier transform) to the frequency domain before application of the algorithm. ‘Perfect E ’ and ‘Perfect H ’ boundary conditions are applied to the xz and yz planes, respectively. These symmetry conditions reduce domain size and increase the overall accuracy of the simulation by permitting a greater density of elements to be employed in the relevant portions of the geometry.

2.2 PEC results

The first step in this study is to identify the near and far-field responses from the aperture in Fig. 1 without any probe present. To isolate geometric effects from material effects, the metallic film is first modeled as a perfect electric conductor (PEC). For all the work presented in this paper, the incident wave has a 1 V/m peak value of the E field (2 V/m peak-to-peak). Figure 3 shows the magnitude of the electric field at one instant in time (or rather phase-space) for a bowtie with $a = b = 150$ nm with incident plane wave with a free space wavelength of $\lambda = 400$ nm (below cutoff) and $\lambda = 800$ nm (above cutoff) polarized in the y -direction (also see Table 1 for cutoff wavelengths). This can be observed by noting the discontinuity at the entrance of the aperture indicating propagation. The calculation shows that for $\lambda = 400$ nm, part of the incident wave is reflected back by the metal film to form a standing wave, and some of the light also couples into a TE mode and propagates through the aperture. The spatial shape of this mode serves to concentrate the energy in the gap region of the aperture. This is

Fig. 4 Near-field response (energy stored in electromagnetic fields and the magnitude of the pointing vector) from PEC bowties of various sizes



appealing because the mode can be used to concentrate the incident energy to a near field spot with dimensions on the same order as the gap on at the exit plane, as shown in previous numerical work on ridge waveguide apertures [4, 11]. The majority of the energy transmitted from the waveguide is stored in evanescent field near the exit plane, however, a small amount of the light does couple to the far-field. In the $\lambda = 800$ nm case all the modes are cutoff and the field is evanescently decaying through the waveguide.

Figure 4 illustrates the spectral dependence of the bowtie's near-field emission on its outline dimensions (a and b). The field is sampled at the center of the aperture on the exit plane (the free-space side of the metal film). The energy stored in the electric and magnetic fields are, $u_E = \varepsilon E^2/2$ and $u_H = \mu H^2/2$, respectively [9]. In a propagating wave, these two quantities are equal; however, this is not necessarily true in an evanescent field [9]. From our near field results, it was found that the energy stored in the electric field is about one order of magnitude higher than that in the magnetic field. The Poynting vector, $\mathbf{P} = \mathbf{E} \times \mathbf{H}$ gives the magnitude of the energy flow and its direction. Figure 4 shows the sum of the energy density stored in the electric and magnetic field and the magnitude of the Poynting vector at the center of the gap in the exit plane for different sized bowtie apertures (all with $a = b$). It is interesting to observe that the peak field intensities in the near-field all occur slightly at wavelengths slightly longer than the cut-off wavelengths listed in Table 1. The peak value of the Poynting vector also decreases for larger apertures (longer wavelengths) relative to the peak value of the potential energy density. The larger near-field intensity at resonance for larger apertures may be explained by the fact that the incident radiation is being concentrated in the gap region and a greater amount of incident energy is harvested by these apertures.

The far-field pattern is calculated by the transforming the fields calculated at the boundaries of the simulation using

the free-space Green's function [10]. A signature of the far-field is that the E field is orthogonal to the H field and scaled by η , the impedance of the medium. This allows easy calculation of the radiated power. The far-field response has both an angular and spectral dependence as shown in Fig. 5(a) and (b), plotted at $\lambda = 500$ and $\lambda = 750$ nm, respectively. To represent the collection of the emitted light by a microscope objective in a far-field measurement, the radiated power is integrated over a collection angle, which is selected to be 27° corresponding to a $50\times$ objective with $\text{NA} = 0.45$. Figure 5(c) shows the far field resonant peaks are closely correlated with the near-field emission of the bowtie aperture.

The next step in this study is to examine if the resonance can be resolved by NSOM measurements. Figure 6 shows the magnitude of the electric field with the presence of an NSOM probe for a bowtie sample with $a = b = 150$ nm. It can be seen that the field is disturbed by the probe and very little of the energy propagates into the probe. To calculate an NSOM signal, the Poynting vector is integrated over the signal plane of the probe as shown in Fig. 2. Figure 7 shows the magnitude of this signal for a probe with a circular aperture and a diameter of 150 nm. The resonant peaks of the various sized bowties are all above the cutoff wavelength of the circular hole in the probe. This leads to the resolution of only the shortest wavelength resonant peaks. The signals are also slightly blue shifted because of the greater sensitivity to shorter wavelengths and therefore better coupling between the bowtie aperture and the probe at shorter wavelengths.

The results shown above also suggest a great spectral sensitivity to the probe dimensions. To illustrate this, the $a = b = 150$ nm bowtie is imaged by probes with apertures of different diameters. Figure 8 shows the calculated signals along with the Poynting vector for the aperture without any probe. The signals were all scaled to unity at 400 nm. It is seen that the holes with larger radius would better resolve the spectral information. However, using a probe with large

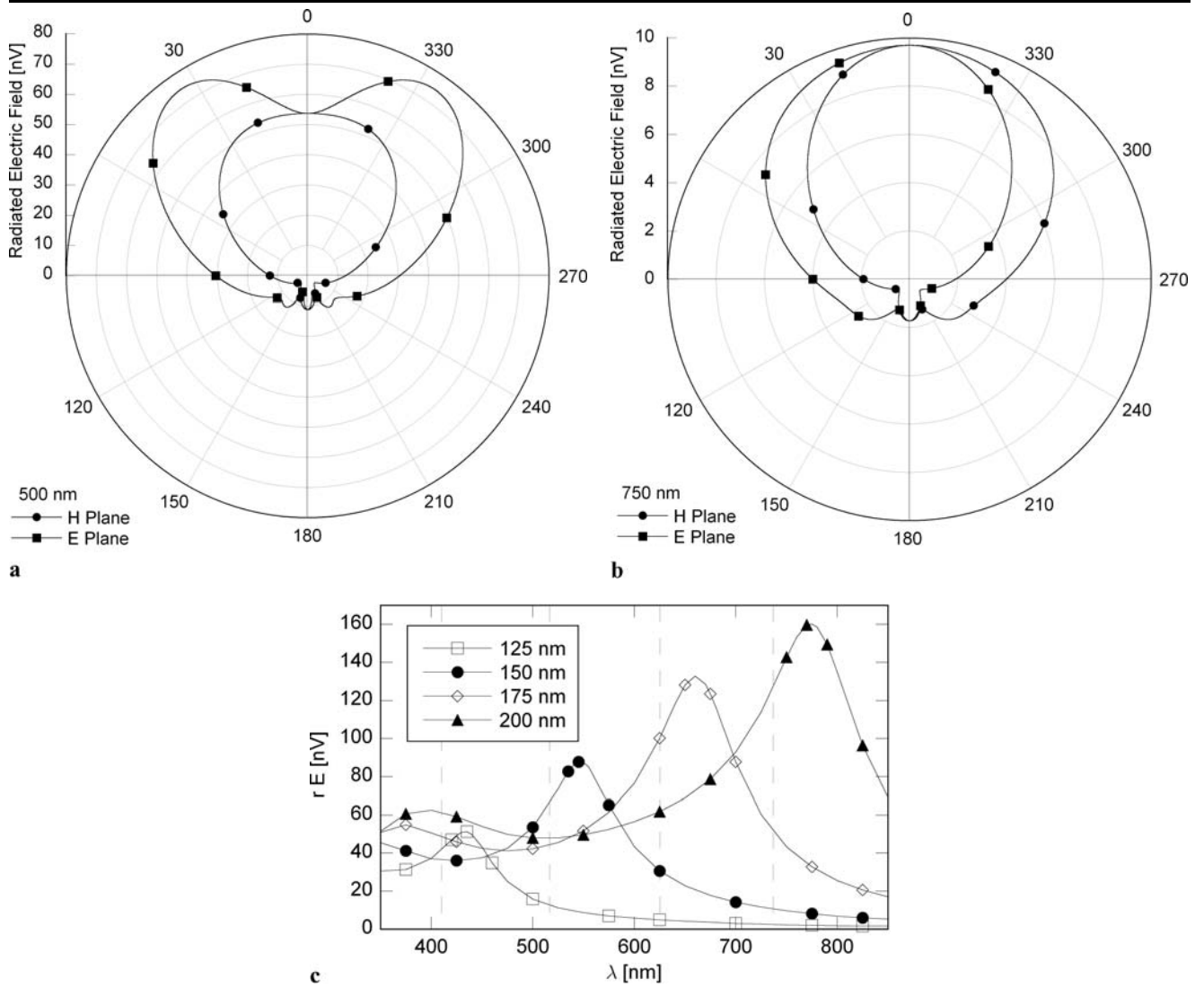
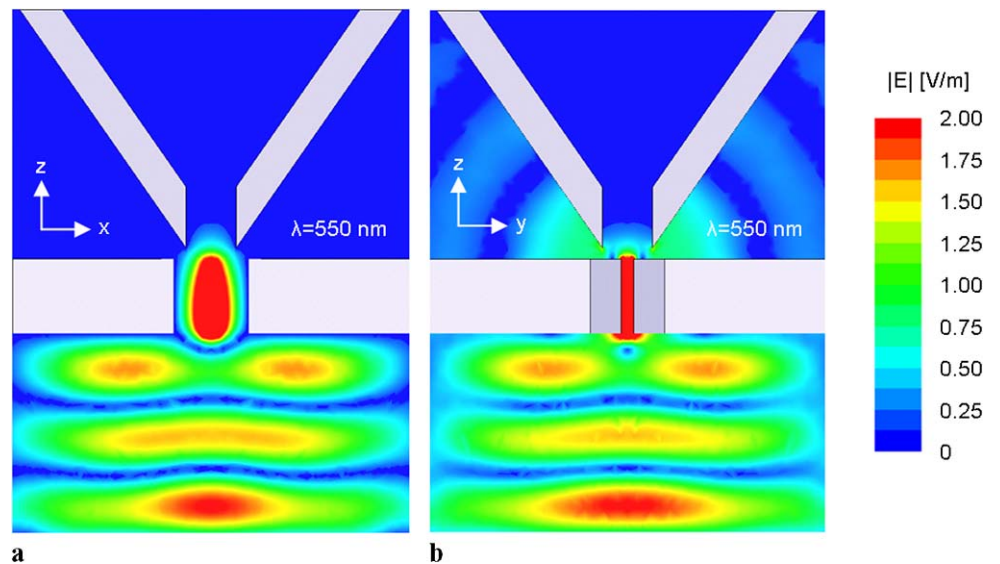


Fig. 5 Far-field patterns for PEC bowtie aperture, $a = b = 150$ nm, (a) below the cutoff wavelength, $\lambda = 500$ nm, (b) above the cutoff wavelength: $\lambda = 750$ nm, along with (c) the radiated E field for different sized bowties at different wavelengths

Fig. 6 Magnitude of E field for 150 nm bowtie examined with a 50 nm hole in the (a) H plane and (b) E plane



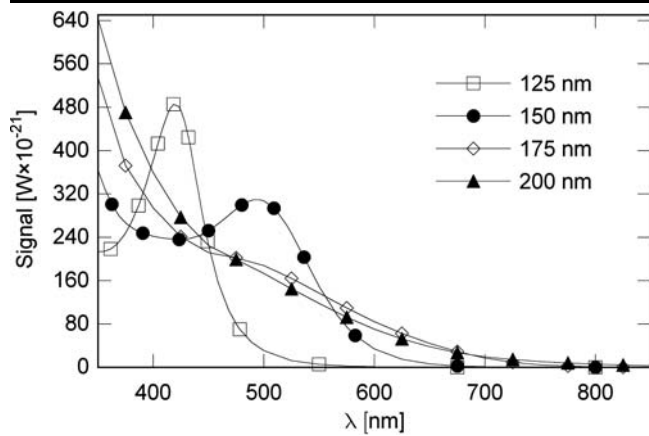


Fig. 7 Response from PEC bowties from NSOM probe with a 75 nm radius hole

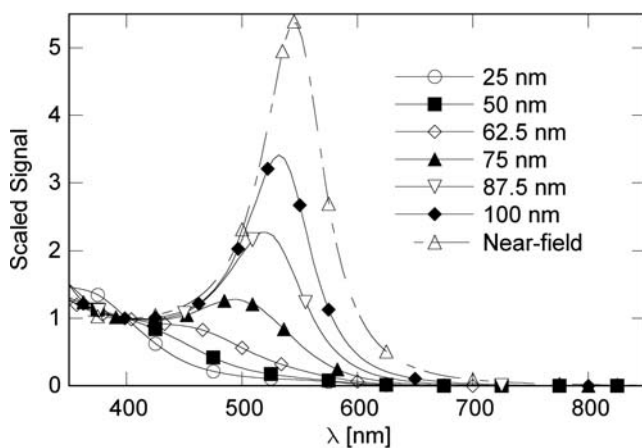
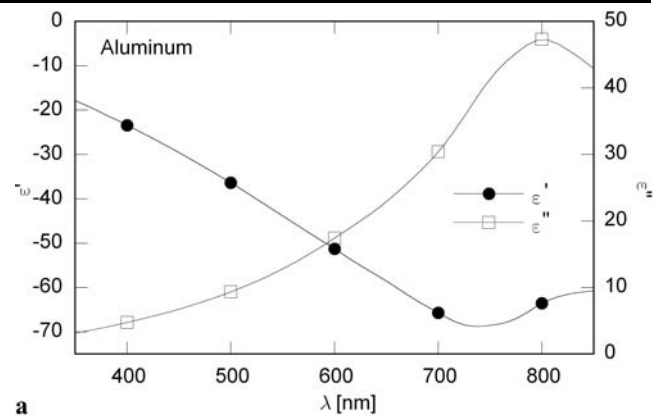


Fig. 8 Signal from different radius probes

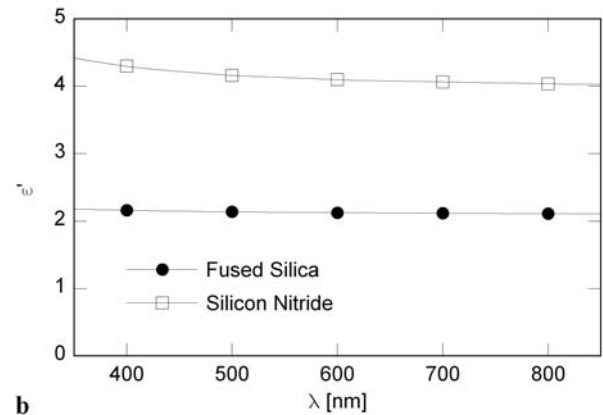
radius will result in a larger sample volume, which will reduce the spatial resolution. It should also be pointed out that there is several orders of magnitude difference between the signals from the 25 and 100 nm radius probes.

2.3 Real materials

At optical wavelengths, the optical properties of metal must be considered as they significantly affect the field distributions. The field penetrates a finite amount into a metal and the conductor introduces a tangible amount of loss. In addition, resonant effects such as surface-plasmons may be an issue [5]. The properties of metal such as aluminum vary significantly over optical wavelengths as can be seen in Fig. 9(a) [12]. By contrast, the dielectric properties for both silicon nitride and quartz [13] do not vary significantly over this interval.



a



b

Fig. 9 Optical properties of (a) aluminum and (b) silicon nitride from [12] and synthetic quartz from [13]

The distance that the fields penetrate into a metal is given by the skin depth of the metal, which is expressed as [10]:

$$\delta = \frac{\lambda}{2\pi \operatorname{Im}(\sqrt{\epsilon})}, \quad (2)$$

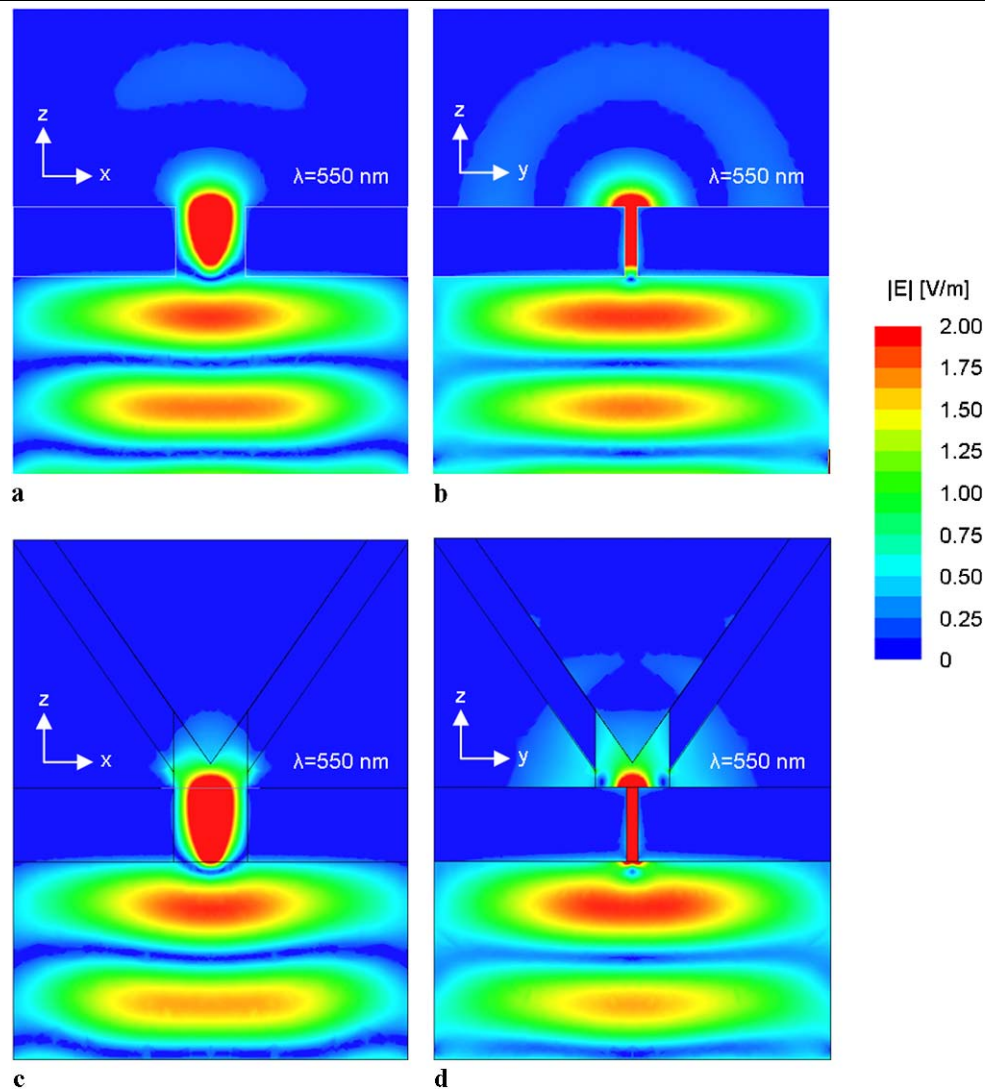
where ϵ is the dielectric function of metal. The field penetration into the metal surface serves to effectively make the aperture's profile larger. The varying imaginary portion of the permittivity as a function of wavelength leads to variable losses given by [9, 10]

$$P_l = R_s \int_C |\mathbf{J}_s|^2 dl, \quad (3)$$

where R_s is the surface resistance of the conductor and \mathbf{J}_s is the surface current given by $\hat{n} \times \mathbf{H}$ on the metal surface. Compared to Figs. 3 and 6, Fig. 10 shows that these effects significantly modify the response of the aperture.

Figures 11(a) and (b) show the response of bowtie apertures with different sizes using properties of aluminum, in the near- and far-field, respectively. The variance of the permittivity shown in Fig. 8 is reflected in both the near and far-fields and the peaks from the PEC model are dra-

Fig. 10 Magnitude of E fields for bowtie 550 nm nanoaperture in 150 nm thick aluminum on the (a) *H* plane and (b) *E* plane, and on the (c) *H* plane and (d) *E* plane with an NSOM probe



matically washed out. This can be attributed to the effects of the varying permittivity of aluminum discussed above.

Figure 12 shows the Poynting vector averaged over the exit plane of an aluminum coated NSOM probe with a 150 nm diameter hole imaging the different sized aluminum bowties shown previously. The initial resonant peak has been dramatically blue shifted and the convolution with the material properties is evident.

Examining Fig. 11(b), it can be seen that the far-field response from the aperture is much closer to the near-field response than that of the simulated NSOM probe measurements. Figures 7 and 8 both show that it will be difficult to resolve the resonant frequency in the near field using a small circularly shaped aperture. Therefore, the far field measurement is a better choice for studying the spectral response of a nanoscale field.

3 Conclusions

The resonance of different sized nanoscale apertures was determined numerically both in the near- and far-fields. For the PEC system these are shown to be discrete peaks and there is a close correlation between the near- and far-fields. However, when trying to resolve these peaks using an NSOM probe, there is a significant attenuation for the longer wavelengths. For real systems, the spectral response is complicated by the field penetration into the metal and the varying permittivity of the metal. These effects can be present in both the sample and probe, complicating the near-field measurements. Finally, it was shown that for ridge nanoscale apertures, the resonant wavelength can be more readily determined from far-field measurements than using an NSOM system.

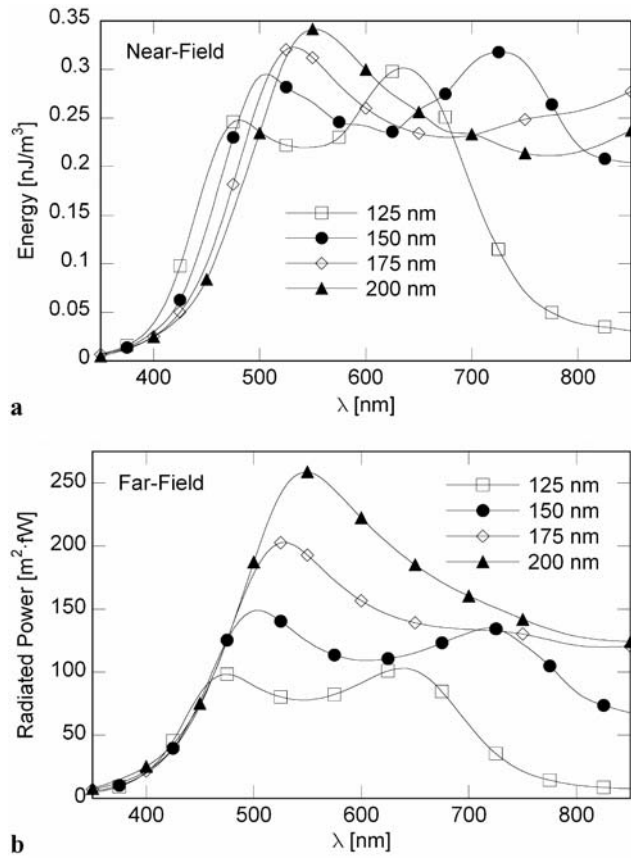


Fig. 11 Potential energy stored in the (a) near field and (b) radiated electric field for different sized apertures in aluminum films

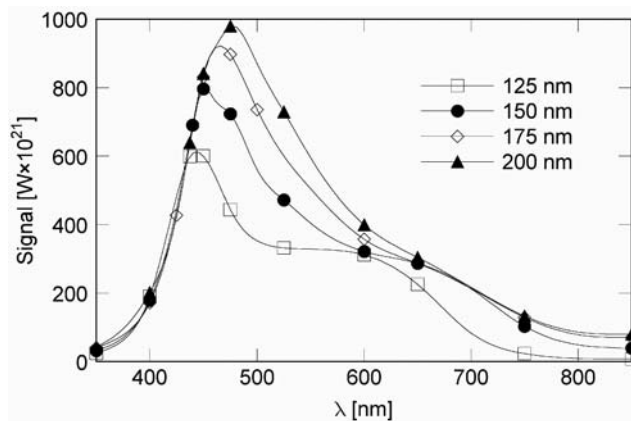


Fig. 12 Signal from different sized bowties using a probe with $r = 75$ nm with aluminum films

Acknowledgements We gratefully acknowledge the funding provided by the National Science Foundation and the Defense Advanced Research Projects Agency. We also greatly appreciate the assistance of Hjalti Sigmarsson and Dr. William Chappell in learning and understanding the HFSS software.

References

1. E.X. Jin, X. Xu, *J. Microscopy* **229**, 503–511 (2008)
2. L. Wang, X. Xu, *Appl. Phys. Lett.* **90**, 261105 (2007)
3. H. Bethe, *Phys. Rev.* **66**, 163–182 (1944)
4. X. Jin, X. Xu, *Jpn. J. Appl. Phys.* **43**, 407–417 (2004)
5. E.X. Jin, X. Xu, *Appl. Phys. B* **84**, 3–9 (2006)
6. K. Şendur, W. Challener, C. Peng, *J. Appl. Phys.* **96**, 2743–2752 (2004)
7. J.A. Matteo, D.P. Fromm, Y. Yuen, P.J. Schuck, W.E. Moerner, L. Hesselink, *Appl. Phys. Lett.* **85**, 648–650 (2004)
8. D.M. Pozer, *Microwave Engineering* (Wiley, New York, 2003)
9. S. Ramo, J.R. Whinnery, T. Van Duzer, *Fields and Waves in Communication Electronics* (Wiley, New York, 1994)
10. Ansoft Inc., HFSS™ high frequency structural simulator, Version 10.1. <http://ansoft.com/products/hf/hfss>
11. X. Shi, L. Hesselink, *Jpn. J. Appl. Phys.* **41**, 1632 (2002)
12. E.D. Palik, *Handbook of Optical Constants of Solids* (Academic Press, New York, 1998)
13. I.H. Malitson, *J. Opt. Soc. Am.* **55**(10), 1205–1209 (1965)